Lawrence Berkeley National Laboratory

Title
Crystal-field level inversion in lightly Mn-doped Sr3Ru2O7

Permalink
https://escholarship.org/uc/item/65h0b4nf

Author
Hossain, M. A.

Publication Date
2008-07-03

Peer reviewed

Crystal-Field Level Inversion in Lightly Mn-Doped $Sr_3Ru_2O_7$

M. A. Hossain,[1] Z. Hu,[2] M. W. Haverkort,[2] T. Burnus,[2] C. F. Chang,[2] S. Klein,[2] J. D. Denlinger,[3] H.-J. Lin,[4] C. T. Chen,[4] R. Mathieu,[5] Y. Kaneko,[5] Y. Tokura,[5] S. Satow,[6] Y. Yoshida,[7] H. Takagi,[6] A. Tanaka,[8] I. S. Elfimov,[1] G. A. Sawatzky,[1] L. H. Tjeng,[2] and A. Damascelli[1,*]

[1]*Department of Physics & Astronomy, University of British Columbia, Vancouver, British Columbia V6T 1Z1, Canada*
[2]*II. Physikalisches Institut, Universität zu Köln, Zülpicher Straße 77, 50937 Köln, Germany*
[3]*Advanced Light Source, Lawrence Berkeley National Laboratory, Berkeley, California 94720, USA*
[4]*National Synchrotron Radiation Research Center, 101 Hsin-Ann Road, Hsinchu 30077, Taiwan*
[5]*Department of Applied Physics, University of Tokyo, Tokyo 113-8656, Japan*
[6]*Department of Advanced Materials Science, University of Tokyo, Kashiwa, Chiba 277-8581, Japan*
[7]*National Institute of Advanced Industrial Science and Technology (AIST), Tsukuba, 305-8568, Japan*
[8]*Department of Quantum Matter, ADSM, Hiroshima University, Higashi-Hiroshima 739-8530, Japan*

.

$Sr_3(Ru_{1-x}Mn_x)_2O_7$, in which 4d-Ru is substituted by the more localized 3d-Mn, is studied by x-ray dichroism and spin-resolved density functional theory. We find that Mn impurities do not exhibit the same 4+ valence of Ru, but act as 3+ acceptors; the extra e_g electron occupies the in-plane $3d_{x^2-y^2}$ orbital instead of the expected out-of-plane $3d_{3z^2-r^2}$. We propose that the $3d - 4d$ interplay, via the ligand oxygen orbitals, is responsible for this crystal-field level inversion and the material's transition to an antiferromagnetic, possibly orbitally ordered, low-temperature state.

.

Ruthenium oxides are a particularly interesting class of materials exhibiting Fermi liquid properties, unconventional superconductivity, ferromagnetism and metamagnetism, antiferromagnetic insulating behavior, and orbital ordering. The richness of this physics is a testament of the intimate interplay between charge, spin, orbital, and lattice degrees of freedom, despite the fact that 4d transition metals (TM) are not considered to induce strong electronic correlations. The radial extend of the 4d wave functions is significantly larger than for TM-3d and even O-2p orbitals. This leads to, on the one end, weaker correlation effects than in 3d TM oxides, and, on the other hand, to an interesting competition between local and itinerant physics. Doping a TM 4d-O 2p host with dilute 3d TM impurities might thus be extremely effective in tuning valence, spin, and, orbital characteristics and, in turn, the macroscopic physical properties. We will explore these ideas in the hotly debated $Sr_3(Ru_{1-x}Mn_x)_2O_7$ family: metamagnetism and a field tuned quantum phase transition were discovered on the pure compound [1–3]; with the inclusion of a few percent of Mn, a metal-insulator transition was observed in transport experiments, and the emergence of a Mott-like antiferromagnetic state was proposed [4].

To address the nature of the metal-insulator phase transition in $Sr_3(Ru_{1-x}Mn_x)_2O_7$ and the role of Mn impurities, we used x-ray absorption spectroscopy (XAS). This is an element and site-specific probe that provides information on the electronic structure of impurities and host atoms separately, as well as on the emergence of magnetic correlations. By performing polarization-dependent XAS experiments, one can study linear dichroism (LD) and magnetic circular dichroism (MCD). While MCD in an externally applied magnetic field is sensitive to the expectation value of the local magnetic moment $\langle \mathbf{M} \rangle$ and is thus a probe of ferromagnetism, LD is proportional to $\langle \mathbf{M}^2 \rangle$ and in turn the nearest-neighbor spin-spin correlation function, thus providing unique information on orbital population
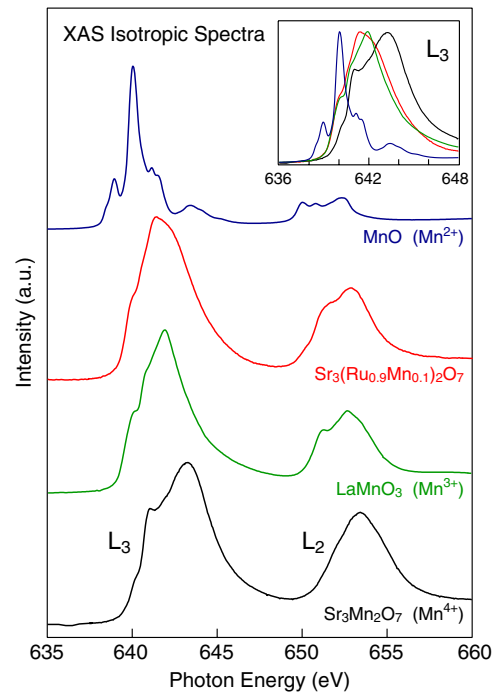

FIG. 1 (color online). Isotropic Mn $L_{2,3}$-edge XAS data from $Sr_3(Ru_{0.9}Mn_{0.1})_2O_7$ and stoichiometric Mn oxides of known valences. Inset: detailed view of the L_3-edge chemical sh

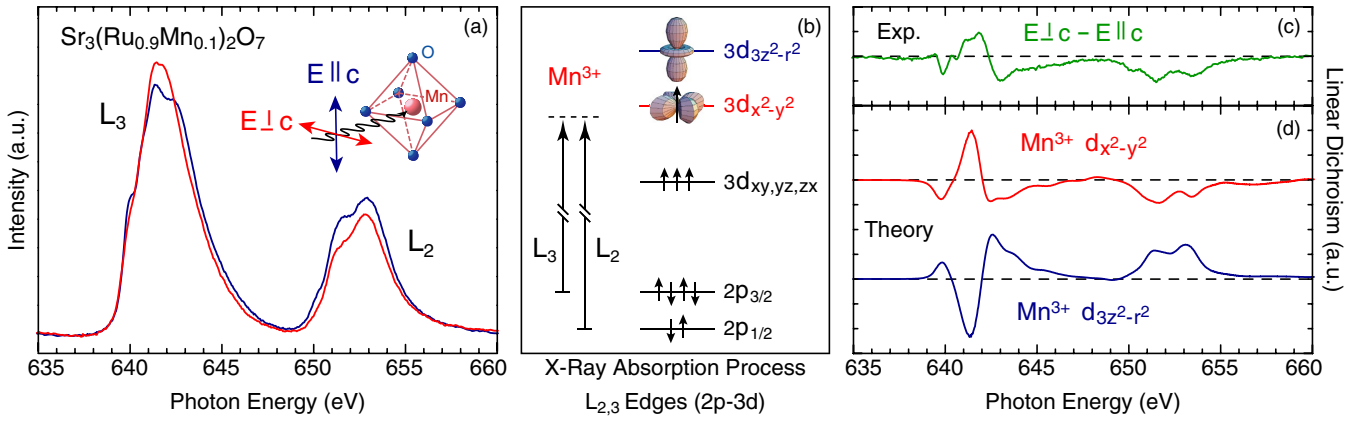FIG. 2 (color online). (a) Polarization-dependent Mn $L_{2,3}$-edge XAS spectra from $Sr_3(Ru_{0.9}Mn_{0.1})_2O_7$ at $T = 295$ K. (b) Scheme of the XAS process: the L_2 (L_3) edge corresponds to the excitation of a Mn $2p_{1/2}$ ($2p_{3/2}$) electron to the Mn $3d$ valence shell. The L_3-L_2 energy separation is due to the $2p$ core level spin-orbit coupling. (c) Corresponding experimental linear dichroism (LD), defined as LD = $[I_{XAS}(\mathbf{E} \perp c) - I_{XAS}(\mathbf{E} \parallel c)]$. (d) Calculated LD spectra for two possible e_g-orbital occupations ($x \parallel a$, $y \parallel b$, $z \parallel c$).

[5,6] as well as antiferromagnetic order [7,8]. We performed temperature-dependent MCD experiments in a 0.5 Tesla field on Mn-doped $Sr_3Ru_2O_7$ for Mn concentration as high as 20%, without detecting any signal above the 2% noise level, which excludes ferromagnetism down to 15 K. In this Letter, we will thus concentrate on room-temperature XAS-LD experiments.

Single crystals of $Sr_3(Ru_{1-x}Mn_x)_2O_7$ were grown by the floating zone technique [4]. Total electron-yield XAS measurements were performed at the Dragon beam line at NSRRC in Taiwan and at beam line 8.0.1 at ALS in Berkeley (the energy resolution was 0.3 eV and the degree of linear polarization ~98%). All sample surfaces were prepared by *in situ* cleaving at pressures better than 2×10^{-9} mbar. The XAS data were normalized to the beam intensity I_0; the absolute energy calibration (with accuracy ~0.02 eV) was obtained from the simultaneous XAS measurement of a MnO single crystal performed in a separate chamber with a small part of the beam [9].

Before discussing the LD results and possible ordering phenomena, we will address the very basic question of what is the valence of Mn in $Sr_3(Ru_{1-x}Mn_x)_2O_7$. The pure compound is ionic with valence Sr^{2+}, Ru^{4+}, and O^{2-}, which would suggest the substitution of Ru^{4+} with Mn^{4+} upon doping. Interestingly, in the related compounds $SrRu_{1-x}Cr_xO_3$ [10] and $CaRu_{1-x}Cr_xO_3$ [11], one might also expect the naive $Ru^{4+} \rightarrow Cr^{4+}$ substitution. However, although the valence was not probed directly, from the anomalous dependence of the unit cell volume on Cr content, a substantial $Ru^{4+} + Cr^{4+} \rightarrow Ru^{5+} + Cr^{3+}$ charge transfer was proposed [10,11]. Thus, in the present case, the 4+ valence of Mn should not be taken for granted but determined experimentally. Room-temperature, isotropic Mn $L_{2,3}$-edge XAS data from 10% Mn-doped $Sr_3Ru_2O_7$ are presented in Fig. 1, together with the results from other Mn-oxide compounds characterized by a well-defined Mn valence, such as MnO (2+), $LaMnO_3$ (3+), and $Sr_3Mn_2O_7$ (4+) [see Fig. 2(b) for a description of the

$L_{2,3}$-edge XAS process]. As shown in Fig. 1, the energy position of the $L_{2,3}$ absorption edge is exquisitely sensitive to the valence of an element. The shift of the center of gravity to high energy upon increasing the Mn valence from 2+ to 4+ (i.e., "chemical shift"), and the very close match between $Sr_3(Ru_{0.9}Mn_{0.1})_2O_7$ and $LaMnO_3$ $L_{2,3}$-edge energy and line shape (inset of Fig. 2), provide already the first surprise: Mn impurities in $Sr_3Ru_2O_7$ act as Mn^{3+} electron acceptors.

The 3+ valence of Mn has important consequences. While Mn^{4+} has three d electrons in the 1/2-filled t_{2g} shell, Mn^{3+} has an extra e_g electron ($t_{2g}^3 e_g^1$) and is Jahn-Teller active, which adds the orbital dimension to the problem. The key question is whether the e_g electron will occupy the in-plane $d_{x^2-y^2}$ or out-of-plane $d_{3z^2-r^2}$ orbital. Since $Sr_3Ru_2O_7$ is a tetragonally distorted system with RuO_6 octahedra elongated along the c-axis, crystal-field splitting would lead to the occupation of the out-of-plane $d_{3z^2-r^2}$ orbital. This intuitive picture can be directly verified by x-ray LD. Room-temperature, linearly polarized Mn $L_{2,3}$-edge XAS spectra from 10% Mn-doped $Sr_3Ru_2O_7$ are presented in Fig. 2(a). The corresponding LD, defined as the difference between XAS spectra acquired with light polarization perpendicular ($\mathbf{E} \perp c$) and parallel ($\mathbf{E} \parallel c$) to the crystal c axis, is shown in Fig. 2(c). Information about the orbital population of Mn e_g levels can be extracted through the detailed comparison between the measured LD and multiplet cluster calculations for different electronic configurations of the Mn, which are shown in Fig. 2(d). As we will discuss below, the multiplet calculations are based on parameters from our *ab initio* density functional theory results (Figs. 3 and 4), and are thus not an arbitrary fit of the data. The two simulated LD spectra are opposite to each other in terms of sign and reveal the in-plane $d_{x^2-y^2}$ orbital polarization for the Mn^{3+} e_g electrons [Fig. 2(b)], instead of the expected $d_{3z^2-r^2}$. Also, the room-temperature LD spectra are virtually indis-

tinguishable for all of the $Sr_3(Ru_{1-x}Mn_x)_2O_7$ samples we studied, indicating that Mn^{3+} valence and $d_{x^2-y^2}$ orbital polarization persist across the whole 5–20% doping range.

This *inversion* of the conventional *crystal-field orbital hierarchy* at Mn impurities in $Sr_3(Ru_{1-x}Mn_x)_2O_7$ is a very surprising result. To illustrate this point, we have performed local-density approximation (LDA) band-structure calculations for undoped $Sr_3Ru_2O_7$ (Ru327) and $Sr_3Mn_2O_7$ (Mn327), with the full-potential linearized augmented plane-wave density functional theory code WIEN2K [12]. In both cases, we have used structural data for Ru327 [13], since our end goal will be that of studying Ru327 for dilute Ru-Mn substitution. As shown in Figs. 3(a) and 3(b), the basic electronic structures for the two stoichiometric compounds is very similar and is set by the overlap of O-2p and TM-d orbitals. However, the Mn-3d orbitals are more spatially localized than the rather extended Ru-4d orbitals; this leads to a reduced bonding-antibonding splitting with the O-2p states and, as clearly evidenced by the in-plane O-2p density-of-states (DOS), to an overall 30% bandwidth reduction in Mn327 as compared to Ru327. As for the states of mainly TM-d character, the t_{2g} band is located within a 1–2 eV range about the chemical potential and is partially occupied (corresponding to a 4+ valence for both Mn and Ru), while the e_g states are higher in energy and completely unoccupied. Most importantly, as summarized in Table I, the first moments of the TM-e_g partial DOS indicate a lower energy for the $d_{3z^2-r^2}$ than $d_{x^2-y^2}$ states in both Ru327 and Mn327, consistent with the standard crystal-field description for elongated $TM-O_6$ octahedra.

To understand the origin of the level inversion observed in $Sr_3(Ru_{1-x}Mn_x)_2O_7$, we have to further our density functional theory study with the inclusion of dilute Mn impurities. The close similarity of Ru327 and Sr_2RuO_4 (Ru214) electronic structures, with almost identical bandwidths [Figs. 3(a) and 3(c)], first moments (Table I), and marginal k_z dispersion (not-shown), suggests that the computationally demanding problem of performing calculations for dilute impurities in bilayer Ru327 can be more efficiently solved in single-layer Ru214 [14] (the main difference between the two is the apical oxygen DOS in Figs. 3(a) and 3(c), which is due to the presence of an additional apical site within the RuO_2 bilayer in Ru327 and is not relevant to the present discussion). We have thus performed spin-polarized calculations (LSDA) for Mn-doped Ru214 with a 3 × 3 supercell in the *ab*-plane (~11% Mn).

As shown by the spin-up e_g Mn DOS in Figs. 4(a) and 4(b), in which Mn-$d_{x^2-y^2}$ is lower in energy than Mn-$d_{3z^2-r^2}$, LSDA calculations do reproduce the crystal-field inversion discovered in $Sr_3(Ru_{1-x}Mn_x)_2O_7$. This result, which as we have seen is specific to the case in which Mn is introduced as an impurity, originates from the interplay between the spatially confined Mn-3d orbitals and the very extended, yet very anisotropic, Ru 4d-O 2p electronic backbone of the Ru-O host. Let us illustrate this unusual behavior on the basis of the qualitative hybridization
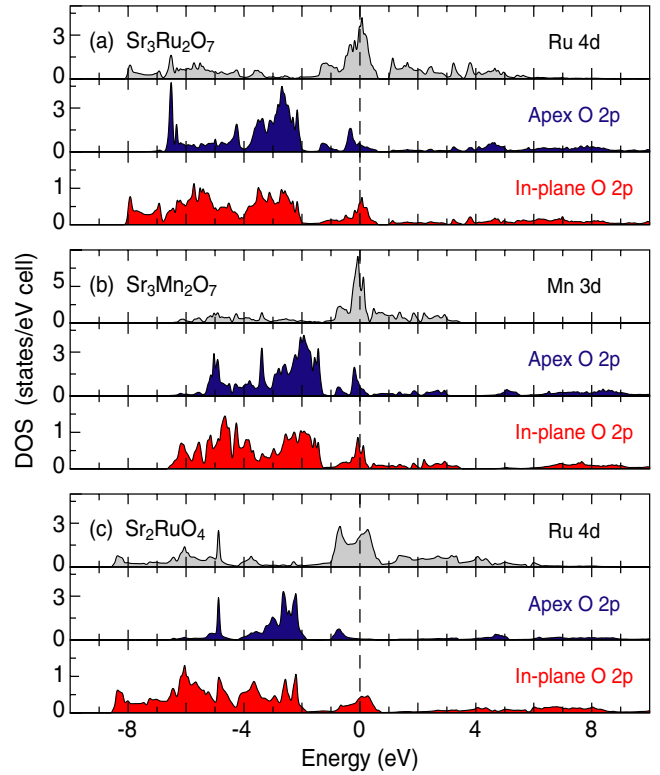

FIG. 3 (color online). Density-of-states (DOS) of stoichiometric (a) $Sr_3Ru_2O_7$ (Ru327), (b) $Sr_3Mn_2O_7$ (Mn327) with the crystal structure of Ru327, and (c) Sr_2RuO_4 (Ru214).

scheme of Figs. 4(c)–4(f). Before the O/Mn-impurity hybridization is turned on [Figs. 4(c) and 4(f)], the Mn e_g orbitals are arranged according to the conventional crystal-field splitting for elongated $TM-O_6$ octahedra, with a small positive difference $\delta = \epsilon_x - \epsilon_z$ for the on-site energies $\epsilon_{x,z}$ of the Mn $d_{x^2-y^2}$ and $d_{3z^2-r^2}$ orbitals. As the hybridization is turned on, however, a level inversion $\Delta_{CF} > 0$ can be realized if $\tau_z^2/\Delta_z - \tau_x^2/\Delta_x > \delta$, where Δ_x (Δ_z) is the on-site energy difference between Mn $d_{x^2-y^2}$ $(d_{3z^2-r^2})$ and in-plane (apical) oxygen ligand orbitals, and τ_x (τ_z) is the in-plane (out-of-plane) O-ligand/Mn-d hybridization parameter. Since $\tau_x > \tau_z$ for elongated octahedra, the level inversion requires $\Delta_x \gg \Delta_z$, which is indeed realized in Mn-doped Ru214 and Ru327 with a few eV

TABLE I. DOS first moments [$\int \omega DOS(\omega)d\omega$] calculated for oxygen molecular orbitals (MO) and transition metal (TM) e_g orbitals with $x^2 - y^2$ and $3z^2 - r^2$ symmetry, for stoichiometric Ru327, Mn327 (in the Ru327 structure), and Ru214. Negative (positive) values identified occupied (unoccupied) states.

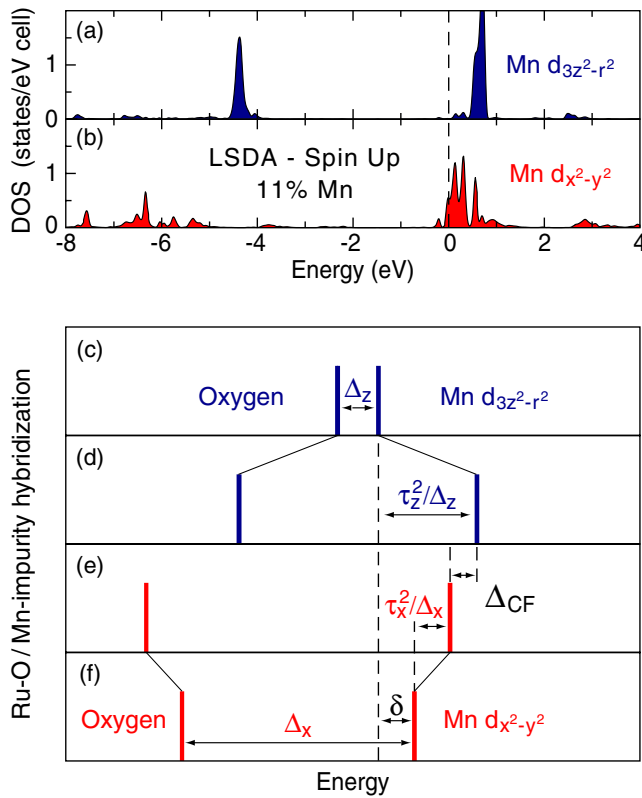| Orbital Symmetry	Ru327 (eV)	Mn327 (eV)	Ru214 (eV)
$TM_{x^2-y^2}$	3.23	1.94	3.20
$TM_{3z^2-r^2}$	2.93	1.82	2.93
$MO_{3z^2-r^2}$	−6.00	−4.20	−5.73
$MO_{x^2-y^2}$	−6.95	−4.94	−7.38

FIG. 4 (color online). (a), (b) Spin-up density of states (DOS) from LSDA calculations for out-of-plane $d_{3z^2-r^2}$ and in-plane $d_{x^2-y^2}$ Mn e_g orbitals in 11% Mn-doped Ru oxides. (c)–(f) Ru-O/Mn-impurity hybridization leading to the Mn orbital hierarchy inversion: energy of (c) out-of-plane and (f) in-plane Mn-impurity and O orbitals in the $Sr_3Ru_2O_7$ host material before the Mn-O hybridization is turned on; (d), (e) once the O/Mn-impurity hybridization is considered, the Mn e_g-orbital hierarchy is inverted ($\Delta_{CF} > 0$) if $\tau_z^2/\Delta_z - \tau_x^2/\Delta_x > \delta$.

difference between Δ_x and Δ_z. Note, however, that although the LSDA calculations of Figs. 4(a) and 4(b) do capture the orbital hierarchy revealed by the present XAS-LD experiments, the location of the Mn $d_{x^2-y^2}$ orbitals right above the chemical potential would still lead to a Mn^{4+} valence. This can be understood as a consequence of the self-interaction that in LDA reduces the ionization energy of localized states more than that of extended states, making it easier for Mn impurities embedded in the Ru-O host to achieve a higher oxidation state. To some extent, the LDA + U scheme takes care of the self-interaction problem, and Mn^{3+} is obtained in calculations with $U_{Mn} > 4$ eV [15].

The findings of our density functional theory study provide an *ab initio* foundation for the ligand field calculations of the Mn multiplet electronic structure and LD spectra presented in Fig. 2(d). These were performed with the program XTLS8.3 [16] and the parameters $U_{dd} = 4.5$, $U_{dp} = 6.0$, $\Delta = 0.5$, $\delta = \epsilon_x - \epsilon_z = 0.2$, and $\tau_{x(z)} = \sqrt{3}pd\sigma_{x(z)}$, all expressed in eV, where U_{dd} and U_{dp} are

the Mn $d - d$ and Mn $d - 2p$ average Coulomb repulsion; Δ is the multiplet average energy difference between the Mn d^4 and the Mn $d^5\underline{L}$ configuration; $pd\sigma_z = -1.2$ eV is the out-of plane O-ligand/Mn-d hopping-integral, which has been taken to be 80% of the in-plane $pd\sigma_x = -1.5$ eV. Finally, the $d_{3z^2-r^2}$ LD spectrum in Fig. 2(d) was calculated with degenerate ligand orbitals, in which case $d_{3z^2-r^2}$ is occupied. The $d_{x^2-y^2}$ LD spectrum is instead obtained with $\Delta_x - \Delta_z = 4.7$ eV, and the close agreement with the experimental LD spectrum [Figs. 2(c) and 2(d)] provides a direct confirmation of our analysis.

We have shown that, at the microscopic level, the remarkable sensitivity of $Sr_3Ru_2O_7$ to light Mn doping stems from the interplay of the localized Mn $3d$ impurity with extended Ru $4d$-O $2p$ orbitals. Clearly, one should include in the calculations also detailed information on the local structure around the Mn impurities: a contraction along the c axis and elongation along a and b axes have been seen by x-ray diffraction across the metal-insulator transition [4], which might imply a compression of the MnO_6 octahedra. Our study indicates that, although such compression would be consistent with—and further enhance—the observed crystal-field level inversion, the driving mechanism for this phenomenon is purely of electronic origin. More generally, the substitution of $3d$-TM impurities in $4d$ and even $5d$ TM oxides might provide a novel, powerful approach to the tailoring of the physical properties of complex oxides.

*damascelli@physics.ubc.ca
[1] R. S. Perry *et al.*, Phys. Rev. Lett. **86**, 2661 (2001).
[2] S. A. Grigera *et al.*, Science **294**, 329 (2001).
[3] R. S. Perry *et al.*, Phys. Rev. Lett. **92**, 166602 (2004).
[4] R. Mathieu *et al.*, Phys. Rev. B **72**, 092404 (2005).
[5] C. T. Chen *et al.*, Phys. Rev. Lett. **68**, 2543 (1992).
[6] D. J. Huang *et al.*, Phys. Rev. Lett. **92**, 087202 (2004).
[7] P. Kuiper *et al.*, Phys. Rev. Lett. **70**, 1549 (1993).
[8] D. Alders *et al.*, Phys. Rev. B **57**, 11623 (1998).
[9] H. Kurata and C. Colliex, Phys. Rev. B **48**, 2102 (1993).
[10] A. J. Williams *et al.*, Phys. Rev. B **73**, 104409 (2006).
[11] V. Durairaj *et al.*, Phys. Rev. B **73**, 214414 (2006).
[12] P. Blaha *et al.*, *An Augmented Plan Wave and Local Orbitals Program for Calculating Crystal Properties*, edited by K. Schwarz (Technical University of Wien, Vienna, 2001).
[13] H. Shaked *et al.*, J. Solid State Chem. **154**, 361 (2000);
[14] O. Chmaissem *et al.*, Phys. Rev. B **57**, 5067 (1998).
[15] I. S. Elfimov and M. W. Haverkort *et al.* (unpublished).
[16] A. Tanaka and T. Jo, J. Phys. Soc. Jpn. **63**, 2788 (1994).